SUPPLEMENTARY INFORMATION

A restricted spectrum of *NRAS* mutations causes Noonan syndrome

Ion C. Cirstea[1], Kerstin Kutsche[2], Radovan Dvorsky[1], Lothar Gremer[1], Claudio Carta[3], Denise Horn[4], Amy E. Roberts[5,6], Francesca Lepri[7], Torsten Merbitz-Zahradnik[1], Rainer König[8], Christian P. Kratz[9,10], Francesca Pantaleoni[3], Maria L. Dentici[7], Victoria A. Joshi[5,11,12], Raju S. Kucherlapati[5], Laura Mazzanti[13], Stefan Mundlos[4], Michael A. Patton[14], Margherita Cirillo Silengo[15], Cesare Rossi[16], Giuseppe Zampino[17], Cristina Digilio[18], Liborio Stuppia[19], Eva Seemanova[20], Len A. Pennacchio[21,22], Bruce D. Gelb[23], Bruno Dallapiccola[7], Alfred Wittinghofer[24], Mohammad R. Ahmadian[1,27], Marco Tartaglia[3,27] & Martin Zenker[25,26,27]

[1]Institute of Biochemistry and Molecular Biology II, Heinrich-Heine University Medical Center, Düsseldorf, Germany. [2]Institut für Humangenetik, Universitätsklinikum Hamburg-Eppendorf, Hamburg, Germany. [3]Dipartimento di Ematologia, Oncologia e Medicina Molecolare, Istituto Superiore di Sanità, Rome, Italy. [4]Institute of Medical Genetics, Charité, University Medicine of Berlin, Germany. [5]Harvard Medical School, Boston, MA, USA. [6]Department of Cardiology, Children's Hospital Boston, MA, USA. [7]Istituto di Ricovero e Cura a Carattere Scientifico-Casa Sollievo della Sofferenza, San Giovanni Rotondo and CSS-Mendel Institute, Rome, Italy. [8]Institute of Human Genetics, University of Frankfurt, Germany. [9]Clinical Genetics Branch, Division of Cancer Epidemiology and Genetics, NCI, Rockville, MD, USA. [10]Department of Paediatrics and Adolescent Medicine, University of Freiburg, Freiburg, Germany. [11]Partners HealthCare Center for Personalized Genetic Medicine, Boston, MA, USA. [12]Department of Pathology, Massachusetts General Hospital, Boston, MA, USA. [13]Dipartimento di Pediatria, Università degli Studi di Bologna, Bologna, Italy. [14]Department of Clinical Genetics, St. Georges Hospital, London, United Kingdom. [15]Dipartimento di Pediatria, Università di Torino, Turin, Italy. [16]UO Genetica Medica, Policlinico S.Orsola-Malpighi, Bologna, Italy. [17]Istituto di Clinica Pediatrica, Università Cattolica del Sacro Cuore, Rome, Italy. [18]Sezione di Genetica Medica, Ospedale "Bambino Gesù", Rome, Italy. [19]Dipartimento di Scienze Biomediche, Università degli Studi "G.d'Annunzio", Chieti, Italy. [20]Institute of Biology and Medical Genetics, Charles University, University Hospital Prague, Prague, Czech Republic. [21]Genomics Division, Lawrence Berkeley National Laboratory, Berkeley, CA, USA. [22]US Department of Energy Joint Genome Institute, Walnut Creek, CA, USA. [23]Center for Molecular Cardiology and Departments of Pediatrics and Genetics and Genomic Sciences, Mount Sinai School of Medicine, New York, NY, USA. [24]Max-Planck-Institute of Molecular Physiology, Department of Structural Biology, Dortmund, Germany. [25]Institute of Human Genetics, University Hospital of Erlangen, University of Erlangen-Nuremberg, Erlangen, Germany. [26]Institute of Human Genetics, University Hospital of Magdeburg, Otto-von-Guericke-University, Magdeburg, Germany. [27]These authors contributed equally as the senior investigators for this project.

Nature Genetics: doi:10.1038/ng.497

TABLE OF CONTENTS

Nature Genetics: doi:10.1038/ng.497

FIGURES AND TABLES

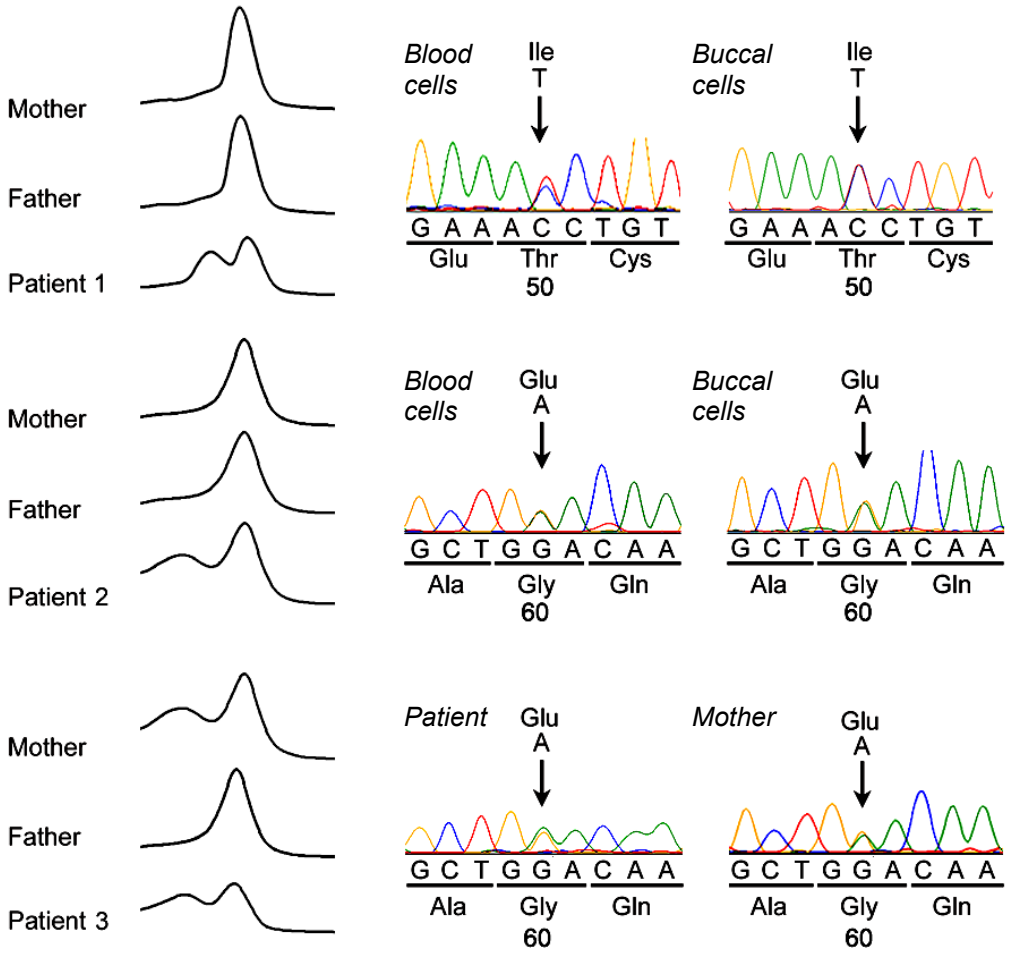

Supplementary Figure 1. Germline *NRAS* mutations cause Noonan syndrome. DHPLC profiles (left) showing the *de novo* origin of the c.149C>T (patient 1) and c.179G>A (patient 2) nucleotide changes in two sporadic cases, and co-segregation of the c.179G>A mutation in a family transmitting the trait (patient 3 and his mother). Sequence electropherograms (right) documenting the heterozygous state for each mutation in peripheral leukocytes, and buccal epithelial cells from individuals 1 and 2, and segregation of the mutation in the heterozygous familial cases (patient 3 and affected mother).

Nature Genetics: doi:10.1038/ng.497

Supplementary Figure 2. Clinical presentation of *NRAS* mutation-positive individuals. Frontal and lateral facial view of patient 1 (4 years old) (**a**,**b**) and whole body aspect of the same individual at age 14 years (**c**,**d**). Note the typical built and thorax deformity. Patient 2 at age 2 years (**e**). Patient 3 at age 6 (**f**) and 20 years (**g**), and his affected mother (50 years old) (**h**). Frontal and lateral facial view of patient 4 (7 years old) (**i**,**j**).

Nature Genetics: doi:10.1038/ng.497

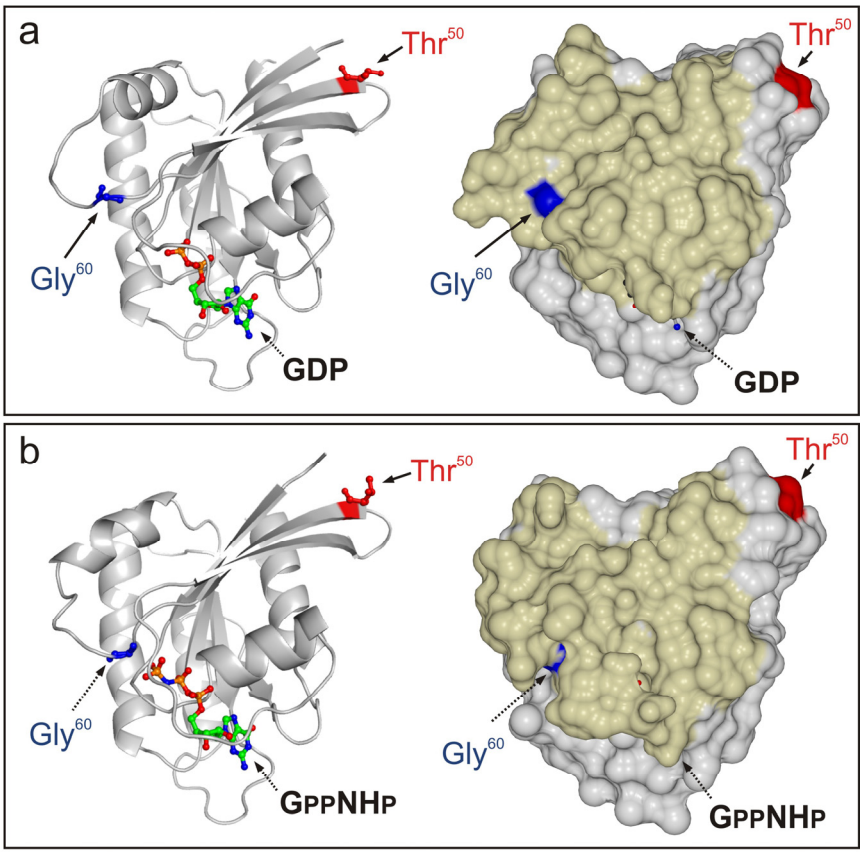

Supplementary Figure 3. Localization of NRAS amino acid residues affected in Noonan syndrome. RAS ribbon structures (left panel) and accessible surfaces (right panel) are shown in the inactive GDP-bound (**a**) and active GppNHp-bound (**b**) states. GppNHp is a non-hydrolysable GTP analog. The contact region of RAS interacting partners (GEFs [catalytic binding site], GAPs and effectors) are highlighted in pale yellow. Thr^{50} (red) and Gly^{60} (blue) are colour-coded. The latter is buried within the hydrophobic core of the protein.

Nature Genetics: doi:10.1038/ng.497

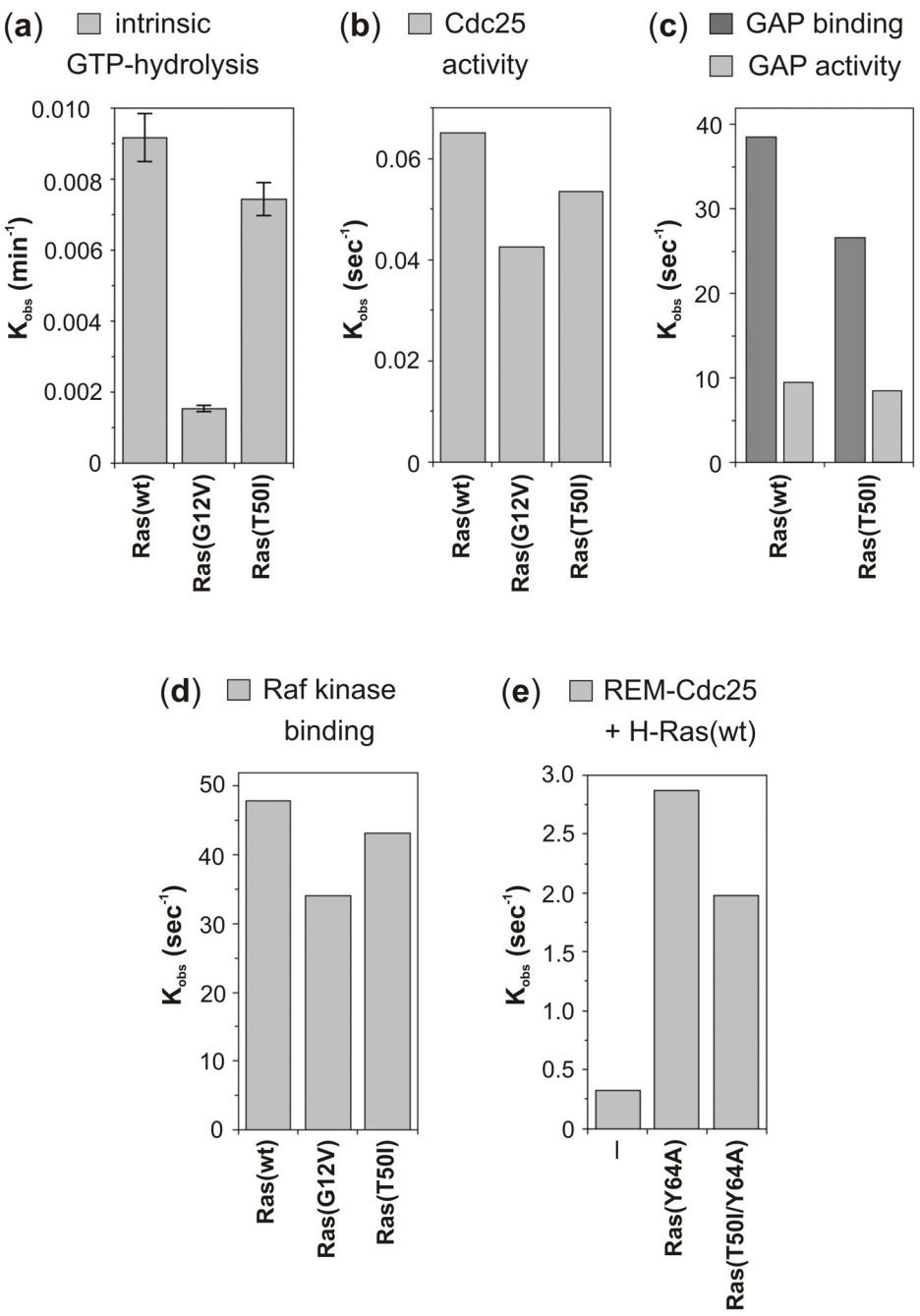

Supplementary Figure 4. Functional assessment of the RAS^{T50I} mutant. (**a**) Intrinsic GTPase activity of wild type RAS, the oncogenic RAS^{G12V}, and Noonan syndrome-causing RAS^{T50I} mutant. [^{32}P]GTP hydrolysis was measured using GTP in a charcoal assay[1]. Observed rate constants (k_{obs}) were obtained from single exponential fitting of data, which are presented as mean values of three independent experiments using 0.6 nM HRAS·[^{32}P]GTP. GTPase activity was substantially impaired in RAS^{G12V} but not in RAS^{T50I}. (**b**) GEF-catalyzed nucleotide release. The fluorescently labelled mGDP release from RAS proteins promoted by the catalytic (CDC25) domain of SOS1 was measured and the mean value of six different experiments was single exponentially fitted to obtain k_{obs} for the reaction of mGDP release

Nature Genetics: doi:10.1038/ng.497

from RAS (0.1 μM) in the presence of 1 μM GEF and 20 μM GDP. The GEF activity was only marginally decreased in both RAS mutants. (**c**) GAP association and stimulated GTP hydrolysis. The catalytic domain of neurofibromin (NF1-333) was used to measure both the association with and GAP-stimulated GTPase activity of wild type RAS and RAS^{T50I} using fluorescently labelled GTP (mGTP)[2]. The mean value of six different stopped-flow experiments was single exponentially fitted to obtain the rates for the association of the GAP (1.5 μM) with RAS·mGTP (0.1 μM) and subsequent stimulation of GTP hydrolysis. GAP-stimulated GTPase activity was normal for RAS^{T50I}, however, a slightly decreased GAP association with RAS^{T50I} was observed. (**d**) Effector association. RAS binding to the RBD of the RAF1 kinase (1 μM) to RAS·mGppNHp (0.1 μM) was measured for wild type RAS and RAS^{T50I}. The mean value of six different experiments was single exponentially fitted to obtain the k_{obs} values for the RAS/RAF1-RBD interaction. RAS^{T50I} revealed almost the same kinetics for the interaction with RAF1 compared with wild type RAS. (**e**) Allosteric activation of SOS1. Thr50 is thought to participate in the interaction network stabilizing RAS binding to the allosteric RAS binding site involving portions of the REM and CDC25 domains of SOS1, which is required for efficient activation of this GEF[3]. The potential perturbing effect of the Noonan syndrome-causing T50I change in allosteric activation of SOS1 was evaluated. Substitution of Tyr^{64} to Ala was used in this assay because in the active GppNHp-bound form RAS^{Y64A} is able to bind the SOS1 allosteric contact site but not the catalytic domain of this GEF[3]. Allosteric activation of SOS1 by binding of GppNHp-loaded forms of RAS^{Y64A} and $RAS^{T50I/Y64A}$ (10 μM) to REM-CDC25 domains of SOS1 (5 μM) was compared by measuring the mGDP release from wild type HRAS (0.2 μM) in the presence of 40 μM GDP. As a control, the nucleotide exchange was measured in the absence of GppNHp-bound proteins (first column). The mean value of six different experiments was single exponentially fitted to obtain k_{obs} for the reaction of mGDP release from RAS. The results indicate that allosteric activation of SOS1 by $RAS^{T50I/Y64A}$ is weaker than that by RAS^{Y64A}, thus providing no explanation for the activating effect of $NRAS^{T50I}$ on the MAPK signaling pathway. Biochemical characterization of the oncogenic and Noonan syndrome-causative mutations was performed on HRAS, which shares 97% amino acid sequence identity with NRAS and exhibits an equivalent structure and functional behaviour.

Nature Genetics: doi:10.1038/ng.497

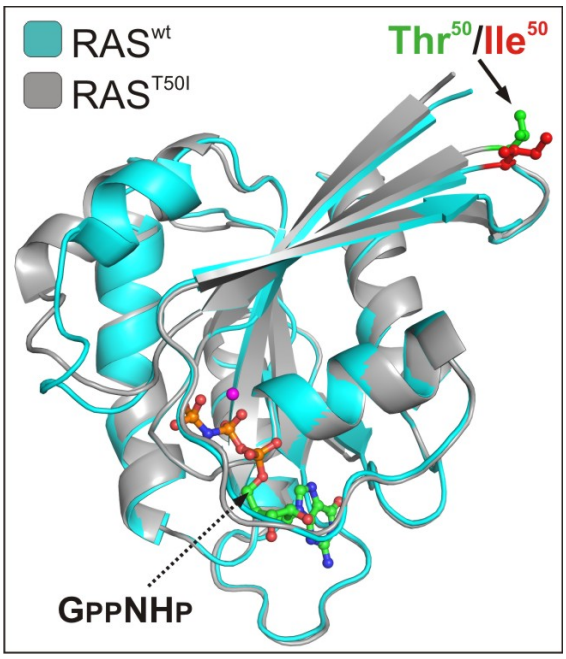

Supplementary Figure 5. Crystal structure of RAS^{T50I} in the active state (cyan ribbon, Supplementary Table 2) overlaid on RAS^{wt} structure (grey ribbon, PDB code 5P21). The Thr^{50} to Ile mutation does not affect considerably the structure. This is obvious from a RMSD (root mean square deviation) of 0.4 Å between Cα backbone atoms. The region encompassing residues 62 to 67 (switch II) exhibits weak electron density indicating large flexibility as frequently observed in previously determined crystal structures of RAS. The conformation of the nucleotide and its contacting residues, as well as the topology of the surface area required for the interaction with GEFs, GAPs and effectors (**Supplementary Fig. 3**) remained unchanged in the T50I mutant and supports the high functional similarity to wild type RAS in the isolated state (**Supplementary Fig. 4**). Bound GppNHp (a non-hydrolysable GTP analog), and the Thr^{50} (green) and Ile^{50} (red) residues are shown as balls and sticks, respectively. Atomic coordinates and structural factors have been deposited within the Research Collaboratory for Structural Bioinformatics (RCSB) Protein Data Bank (PDB) under the accession code 3I3S.

Nature Genetics: doi:10.1038/ng.497

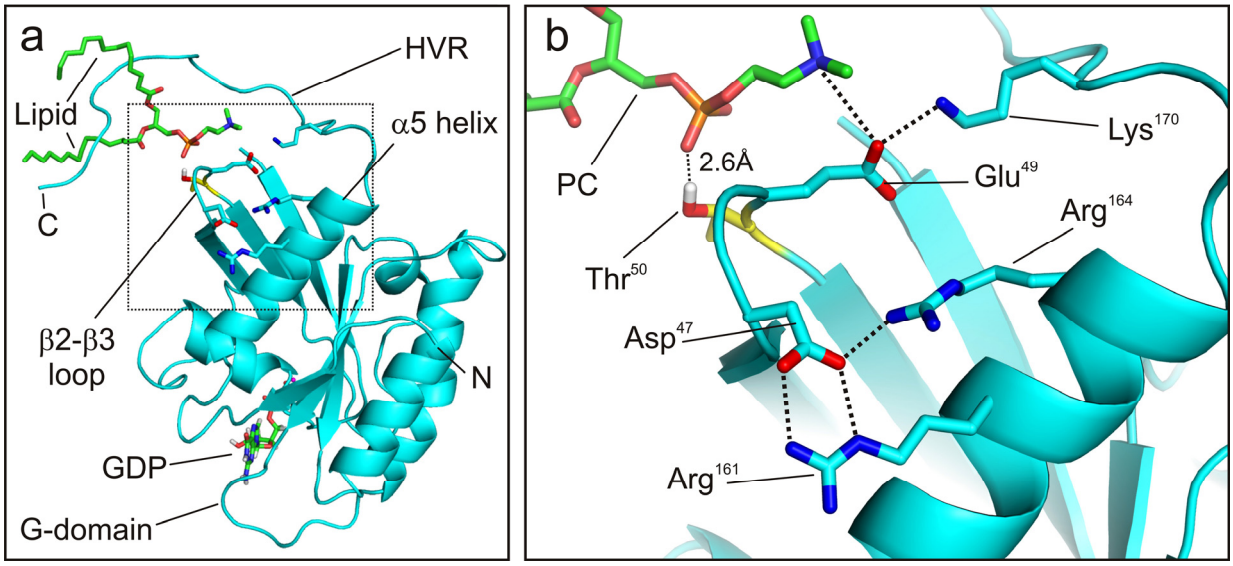

Supplementary Figure 6. Thr^{50} of RAS directly contacts the lipid membrane and participates in a novel switch mechanism that includes residues within the β2-β3 loop and helix α5 to modulate NRAS membrane-orientation. (**a**) GDP-bound HRAS (cyan ribbon) interacting with the membrane (represented for clarity by one lipid molecule, i.e. phosphatidylcholine) was modelled by molecular dynamics simulation according to Abankwa et al.[4]. The hypervariable region (HVR) along with the β2-β3 loop and helix α5 of the GDP/GTP-binding domain (G-domain) of HRAS are shown. The hydrophobic region of the lipid is shown in green, while the phosphate and amine groups are indicated in orange and blue, respectively. (**b**) Magnified view showing Thr^{50} interaction (side chain in yellow, OH in red and white) with a phosphate group of phosphatidylcholine (PC) (cytoplasmic side of the membrane). This interaction is predicted to reinforce an hydrogen bonding network (dashed lines) involving the RAS β2-β3 loop (Asp^{47} and Glu^{49}), helix α5 (Arg^{161} and Arg^{164}) and HVR (Lys^{170}) and the membrane lipid, favouring stabilization of the RAS orientation that is predicted to decrease downstream signalling, presumably by keeping the GTPase in a less productive signaling conformation. Based on this model, the T50I substitution would thus enhance downstream signalling, presumably by destabilizing such an interaction and, consequently, keeping the protein in a more productive signaling conformation.

Nature Genetics: doi:10.1038/ng.497

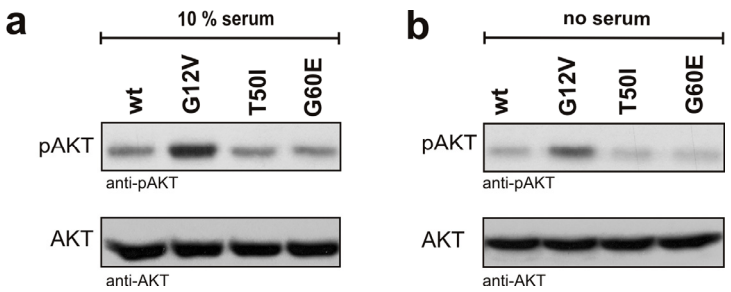

Supplementary Figure 7. AKT phosphorylation levels (replication blot). Independent replication blot showing AKT phosphorylation levels in transiently transfected COS-7 cells cultured in medium with serum (**a**) or in basal medium (**b**). Similar to what is shown in **Figure 2a-b**, only the expression of $NRAS^{G12V}$ resulted in increased AKT phosphorylation, while no effect was detectable in cells expressing the Noonan syndrome-causing $NRAS^{T50I}$ or $NRAS^{G60E}$ mutant under both culture conditions. Note the absence of any additional bands in both pAKT blots, thus confirming the artifactual nature of the additional bands displayed in **Figure 2b**. Total amount of AKT in cell lysates is shown as control.

Nature Genetics: doi:10.1038/ng.497

Supplementary Table 1: Clinical features of patients with Noonan syndrome caused by *NRAS* mutations.

Patient #	**1**	**2**	**3**	**3M**	**4**
NRAS mutation	T50I	G60E	G60E	G60E	T50I
Sporadic / Familial NS	Sporadic	Sporadic	Familial	Familial	Sporadic
Origin of mutation	*de novo*	*de novo*	inherited	N.D.	*de novo*
Paternal age at conception	50 years	31 years	47 years	44 years	34 years
Age	14 years	3.3 years	20 years	50 years	7 years
Sex	Male	Female	Male	Female	Male
Prenatal findings	Nuchal edema, polyhydramnios	Single umbilical artery	No	No	Polyhydramnios
Congenital heart defect	HCM	PS, mitral valve dysplasia, mild HCM	No	No	PS
Rhythm disturbance	SVES	No	No	No	No
Typical facial features	Yes	Yes	Yes	Yes	Yes
Short stature	10^{th} centile*	$<3^{rd}$ centile	$>10^{th}$ centile	10^{th} centile	$<3^{rd}$ centile
Macrocephaly	Yes	No	Yes	Yes	No (relative)
Pterygium colli / webbed neck	Yes	Yes	Yes	Yes	No
Thorax deformity	Yes	Pectus excavatum	Yes	Yes	No
Easy bruising	No	No	No	No	No
Postnatal lymphedema	No	No	No	No	No
Cryptorchidism	Yes	-	Yes	-	Yes
Ophthalmological problems	Myopia	No	No	Myopia	No
Motor delay / muscular hypotonia	Mild	Yes	Yes	Yes	Yes
Mental development	Normal	Speech delay	Normal - borderline	Normal	Borderline
Keratosis pilaris / hyperkeratosis	Severe	Yes	Yes	Yes	No
Hair abnormalities	Curly hair	Sparse thin hair	Curly hair	No	Curly hair
Lentigines / café-au-lait spots	No	No	No	No	No
Myeloproliferative disease	No	No	No	No	No
Other	Pes equinovarus	Palpebral ptosis	Ichthyosiform eczema, acanthosis nigricans, scoliosis	Mother of Pat. 3	

* received growth hormone treatment from the age of 8 years when partial growth hormone deficiency had been noted.
HCM, hypertrophic cardiomyopathy; N.D., not determined; PS, pulmonic stenosis; SVES, supraventricular extrasystoles.

Nature Genetics: doi:10.1038/ng.497

Supplementary Table 2: Crystal parameters, data collection and refined statistics of RAS^{T50I}.

Crystal parameters	
Space group	H32
Cell constants	a = b = 89.21Å; c = 134.64Å;
Data collection	
Beamline	PX-II SLS
Wavelength (Å)	1.0
Resolution range (Å)	99-1.36
No. of observations	368133
No. of unique reflections	44357
Completeness (%)[a]	99.8 (99.9)
R(%)[a]	4.3 (29.5)
I/σ(I)[a]	25.4 (4.6)
Refinement	
Resolution range (Å)	30.8-1.36
No. of reflections test set	2218
No. of non-hydrogen atoms	1609
No. of solvent water	117
R_{work}/R_{free} (%)	16.5/18.3
Average B-factor (Å^2)	13.12
RMSD from ideal geometry	
Bond length (Å)	0.008
Bond angles (°)	1.2
Ramachandran plot (%)[b]	93.1/6.9/0.0

[a]The values in parentheses are calculated in for last resolution shell (1.40-1.36 Å).
[b]Proportion of residues in favored/allowed/outlier region

Nature Genetics: doi:10.1038/ng.497

METHODS

Patients

We obtained DNA samples from unrelated patients with NS (n= 733), CFCS (n= 47) or a phenotype suggestive of these disorders (n= 137), who had been tested negative for mutations in previously identified disease genes (*PTPN11*, *KRAS*, *SOS1*, *RAF1*, *BRAF*, *MEK1* and *MEK2*), and who were ascertained and followed at eight large genetic centers (Berlin, Boston, Erlangen, Hamburg, Rome-Università Cattolica del Sacro Cuore, Rome-Istituto Mendel/Ospedale "Bambino Gesù", Turin and Bologna). The clinical diagnosis was made on the basis of standardized clinical criteria assessed by experienced clinical geneticists. Genomic DNA from blood, skin fibroblasts, hair bulbs and/or epithelial cells from the oral mucosa was extracted using standard protocols. Samples were collected under research projects approved by the Review Boards of all participating institutions, with informed consent. Permission was obtained to publish the photographs of subjects shown in **Supplementary Figure 2**.

Genotyping

Mutational screening of the entire coding sequence of *NRAS* was carried out by denaturing high-performance liquid chromatography (DHPLC) and/or direct bidirectional sequencing of the entire coding region (exons 2 to 5). Primer pairs, PCR and DHPLC conditions are available on request. DHPLC was performed using the 3100 or 3500HT WAVE DNA fragment analysis system (Transgenomic, Omaha, NE). Sequence analysis was carried out by direct, bidirectional sequencing of purified PCR products (Microcon PCR, Millipore, Billerica, MA) using the ABI BigDye Termintor Sequencing Kit v1.1 (Applied Biosystems, Foster City, CA) and an ABI 3730 Capillary Array Sequencer or ABI Prism 310 Genetic Analyzer (Applied Biosystems). Paternity was confirmed in the patients with *de novo* mutations by testing of 16 polymorphic microsatellite markers (Powerplex™, Promega) or using the AmpDESTER Profiler Plus kit (Applied Biosystems).

Nature Genetics: doi:10.1038/ng.497

NRAS expression constructs

NRAS cDNA was cloned in the pEYFP-c1 vector via *Xho*I and *Bam*HI endonuclease digestion. *NRAS* and *HRAS* were used as templates to introduce the Noonan syndrome-causing *NRAS* mutations using a polymerase chain reaction (PCR)-based site-directed mutagenesis protocol as described[6]. The catalytic domain of neurofibromin, NF1-333 (amino acids 1198-1531), was cloned in pGEX-4T-1 via *Eco*RI and *Not*I digestion. Gene segments encoding the RAS binding domain of RAF1 (RAF1-RBD) and the catalytic domain of SOS1 (CDC25) were cloned in the pGEX vectors as described[7,8].

Proteins and fluorescent nucleotides

Wild type RAS and RAS^{T50I} mutant (residues 1-166) were prepared from *Escherichia coli* using an expression system as described[5]. Loading of RAS proteins with GppNHp (a non-hydrolyzable GTP analog) was achieved by incubation of 20 mg RAS protein (0.5 to 1 mM) with a 3-fold molar excess of GppNHp and 60 U alkaline phosphatase (rAPid alkaline phosphatase, Roche, Mannheim, Germany) in standard buffer (30 mM Tris pH 7.5, 5 mM $MgCl_2$, 3 mM dithioerythritol (DTE) containing 200 mM $(NH_4)_2SO_4$ and 100 µM $ZnCl_2$ for 16 h at 4°C[9]. Unbound nucleotides and alkaline phosphatase were removed by gel filtration on a Superdex 75 column (GE Healthcare, Munich, Germany) in standard buffer. GppNHp loading was confirmed by isocratic ion pair reversed phase HPLC on a C-18 column[9]. The nucleotide-free form of RAS and the fluorescent derivatives of GDP, GTP and GppNHp (mantGDP, mantGTP and mantGppNHp) were synthesized as previously reported[10]. RAS·mantGDP, RAS·mantGTP and RAS·mantGppNHp were prepared as described[9]. RAF1-RBD, CDC25 and NF1-333 were produced as glutathione S-transferase (GST) fusion proteins in *Escherichia coli*. All proteins were purified as described previously[10].

Nature Genetics: doi:10.1038/ng.497

Intrinsic GTP hydrolysis

[$^{32}\gamma$]GTP hydrolysis of the RAS proteins (1 μM RAS·GTP contained 6 nM [$^{32}\gamma$]GTP) was analyzed in a buffer containing 30 mM Tris pH 7.5, 10 mM $MgCl_2$, 3 mM DTE at 25 °C by determining the release of radioactive [$^{32}\gamma$]Pi in a charcoal assay. Time-course monitoring of radioactive Pi release was fitted using single exponential equations. Observed rate constants (k_{obs}) were obtained by single exponential fitting of the data.

GEF-catalyzed nucleotide dissociation

GEF-catalyzed mGDP dissociation from the RAS proteins (0.2 μM) was measured in a buffer containing 30 mM Tris pH 7.5, 10 mM KP_i, 5 mM $MgCl_2$ and 3 mM DTE at 25°C in the presence of CDC25 (1 μM), and 40 μM GDP using an Applied-Photophysics stopped flow apparatus. Observed rate constants (k_{obs}) were obtained by single exponential fitting of the data. The impact of the NRAS mutation T50I on allosteric regulation of REM-CDC25 protein of SOS1 was determined under the same condition, by measuring the activity of the CDC25 domain. Specifically, 5 μM GppNHp-bound NRAS mutants in the background of Y64A, which was disabled in the nucleotide exchange reaction, were used. The dissociation of mGDP from wild type RAS was subsequently measured.

GAP-stimulated GTP hydrolysis

For the determination of the rates of NF1-333-stimulated hydrolysis of mGTP bound to RAS, mutants were exchanged with an excess of mGTP in the presence of EDTA to result in a load of higher than 95%. Excess mant-nucleotide was removed by gel filtration and RAS was immediately snap frozen in liquid nitrogen to avoid unmonitored hydrolysis[9]. The exchanged RAS mutant enzymes were reacted in a stopped flow experiment in a buffer containg 30 mM Tris pH 7.5, 10 mM KP_i, 5 mM $MgCl_2$ and 3 mM DTE at 25°C. A final concentration of 300 nM of RAS and 3 μM NF1-333 was used. The reactions showed an initial increase of fluorescence due to association of the GAP domain with the

Nature Genetics: doi:10.1038/ng.497

mant-fluorophore, and a subsequent hydrolysis of mGTP, which was described by a decrease of fluorescence. This decrease, we fitted by a single exponential.

Effector association

RAF1-RBD (1 μM) was used to analyze the impact of T50I in mantGppNHp-bound RAS (0.1 μM) on effector association using an Applied-Photophysics stopped flow apparatus[10]. The mean value of six different experiments was single exponentially fitted to obtain an observed rate constant (k_{obs}) of the RAS/RAF1-RBD interaction.

Cell culture, transient transfection, EGF stimulation, GST pull down and MEK, ERK, AKT activation assays

COS-7 cells were grown in DMEM supplemented with 10 % fetal bovine serum (FBS, Invitrogen) and transiently transfected using DEAE-dextran as described[11]. After transfection, cell cultures were maintained (a) in the presence of 10% FBS for ~42 h (plus serum) or (b) first in the presence of 10% FBS for 22 h and then starved for 20 h (no serum). To determine the effects of EGF stimulation on MAPK signaling, COS-7 cells transfected with different *NRAS* constructs (wild type and mutants) were treated with recombinant EGF (Calbiochem) at different concentrations and harvested at different time points. After optimization, ERK activation was determined upon stimulation of cells with an EGF concentration of 20 ng/ml for 2 min. RAS·GTP levels were determined using GST-tagged RAF1-RBD to pull down active GTP-bound RAS from cellular lysates by glutathione beads (Protino Glutathione Agarose 4B, Macherey-Nagel). The cell lysates were incubated with glutathione beads coupled to GST-tagged RAF1-RBD and were washed four times with buffer (50mM Tris/HCl pH 7.5, 100 mM NaCl, 1% Igepal CA-630, 10% glycerol, 20 mM β-glycerolphosphate, 1 mM Na-orthovanadate, EDTA-free inhibitor cocktail 1 tablet/50 ml) and subjected to SDS-PAGE (15% polyacrylamide). RAS proteins were detected by western blot using a monoclonal antibody against RAS (anti-RAS antibody,

Nature Genetics: doi:10.1038/ng.497

clone Ras10, Millipore). Differentiation of endogenous RAS from ectopically expressed YFP-tagged NRAS proteins was achieved through their different molecular weights (21 kDa versus 38 kDa). Amounts of MEK1/2, ERK1/2, AKT, phospho-MEK1/2, phospho-ERK1/2 and phospho-AKT were determined by western blotting of the same COS-7 cell lysates used for the RAS pulldown assay. Proteins were separated by SDS-PAGE (10% polyacrylamide) and detected by western blotting using antibodies against MEK1/2 (Cell Signaling), ERK1/2 (Cell Signaling), AKT (Cell Signaling), phospho-MEK1/2 (Ser 217/221, Cell Signaling), phospho-ERK1/2 (Thr202/Tyr204, Cell Signaling) and phospho-AKT (Ser473, Cell Signaling).

Crystallization

Crystallization of GppNHp-bound RAS^{T50I} was achieved in a hanging drop vapor diffusion setup at 12°C by mixing 2.5 µl protein (15 mg ml^{-1} in standard buffer) with 2.5 µl reservoir solution consisting of 17% (w/v) PEG 6000, 200 mM $CaCl_2$. Crystals (0.2 x 0.1 x 0.1 mm) were harvested in reservoir solution with 20% glycerol and flash frozen in liquid nitrogen.

Data collection, processing and model building

Data collection was performed at beamline PX-II of the Swiss Light Source (Paul Scherrer Institut, Villigen, Switzerland) at a wavelength of 1.0 Å. Data were processed with XDS.[10] Indexing of the data revealed a unit cell of 89.21 Å, 89.21 Å, 134.64 Å belonging to space group H32 with one RAS molecule in the asymmetric unit (**Supplementary Table 2**). The structure of RAS^{T50I} was solved to near atomic resolution (1.36 Å) by molecular replacement using MOLREP[11] with wild type HRAS (Protein Data Bank code 5P21) as the search model. Refinement of the model was performed with REFMAC[12], followed by TLS refinement[12] of the manually interpreted electron density (COOT)[13].

Nature Genetics: doi:10.1038/ng.497

Web Resources

Accession numbers and URLs for data presented herein are as follows:

Online Mendelian Inheritance in Man (OMIM), http://www.ncbi.nlm.nih.gov/Omim/ (for Noonan syndrome, CFC syndrome, and Costello syndrome);

Gene, http://www.ncbi.nlm.nih.gov/entrez/query.fcgi?db=gene (for *NRAS* cDNA sequences [NM_002524], *HRAS* [NM_005343 and NM_176795], and *KRAS* [NM_033360 and NM_004985]);

Protein Data Bank (PDB), http://pdbbeta.rcsb.org/pdb/Welcome.do (for GDP-HRAS [code 4Q21] and GTP-HRAS [code 5P21] crystal structures);

Catalogue Of Somatic Mutations In Cancer (COSMIC), http://www.sanger.ac.uk/genetics/CGP/cosmic/ (for somatic mutations observed in *NRAS*, *HRAS* and *KRAS*).

Nature Genetics: doi:10.1038/ng.497

References

1. Ahmadian, M.R., Mittal, R., Hall, A. & Wittinghofer, A. Aluminum fluoride associates with the small guanine nucleotide binding proteins. *FEBS Lett* **408**, 315-8 (1997).
2. Ahmadian, M.R., Hoffmann, U., Goody, R.S. & Wittinghofer, A. Individual rate constants for the interaction of Ras proteins with GTPase-activating proteins determined by fluorescence spectroscopy. *Biochemistry* **36**, 4535-41 (1997).
3. Margarit, S.M. et al. Structural evidence for feedback activation by Ras.GTP of the Ras-specific nucleotide exchange factor SOS. *Cell* **112**, 685-95 (2003).
4. Abankwa, D. et al. A novel switch region regulates H-ras membrane orientation and signal output. *EMBO J* **27**, 727-35 (2008).
5. Tucker, J. et al. Expression of p21 proteins in Escherichia coli and stereochemistry of the nucleotide-binding site. *EMBO J* **5**, 1351-8 (1986).
6. Ahmadian, M.R., Stege, P., Scheffzek, K. & Wittinghofer, A. Confirmation of the arginine-finger hypothesis for the GAP-stimulated GTP-hydrolysis reaction of Ras. *Nat Struct Biol* **4**, 686-9 (1997).
7. Herrmann, C., Martin, G.A. & Wittinghofer, A. Quantitative analysis of the complex between p21ras and the Ras-binding domain of the human Raf-1 protein kinase. *J Biol Chem* **270**, 2901-5 (1995).
8. Lenzen, C., Cool, R.H. & Wittinghofer, A. Analysis of intrinsic and CDC25-stimulated guanine nucleotide exchange of p21ras-nucleotide complexes by fluorescence measurements. *Methods Enzymol* **255**, 95-109 (1995).
9. Gremer, L., Gilsbach, B., Ahmadian, M.R. & Wittinghofer, A. Fluoride complexes of oncogenic Ras mutants to study the Ras-RasGap interaction. *Biol Chem* **389**, 1163-71 (2008).
10. Ahmadian, M.R., Wittinghofer, A. & Herrmann, C. Fluorescence methods in the study of small GTP-binding proteins. *Methods Mol Biol* **189**, 45-63 (2002).
11. Herbrand, U. & Ahmadian, M.R. p190-RhoGAP as an integral component of the Tiam1/Rac1-induced downregulation of Rho. *Biol Chem* **387**, 311-7 (2006).
12. Murshudov, G.N., Vagin, A.A. & Dodson, E.J. Refinement of macromolecular structures by the maximum-likelihood method. *Acta Crystallogr D Biol Crystallogr* **53**, 240-55 (1997).
13. Emsley, P. & Cowtan, K. Coot: model-building tools for molecular graphics. *Acta Crystallogr D Biol Crystallogr* **60**, 2126-32 (2004).

Nature Genetics: doi:10.1038/ng.497